A Test of the Continuous Configuration Time-Dependent Self-Consistent Field (CC-TDSCF) Method on the H + CH_4 Reaction†

Liling Zhang,‡ Soo-Y. Lee,§ and Dong H. Zhang*,‡,||

Department of Computational Science, National University of Singapore, Kent Ridge, Singapore 119260, Division of Chemistry & Biological Chemistry, School of Physical and Mathematical Sciences, Nanyang Technological University, 1 Nanyang Walk, Singapore 637616, and Center for Theoretical & Computational Chemistry and State Key Laboratory of Molecular Reaction Dynamics, Dalian Institute of Chemical Physics, Chinese Academy of Sciences, Dalian, P.R. China 116023

Received: November 15, 2005; In Final Form: January 11, 2006

The continuous configuration time-dependent self-consistent field (CC-TDSCF) method is employed to calculate the flux−flux autocorrelation functions for the H + CH_4 reaction on the potential energy surface recently developed by Manthe and co-workers. We include up to 10 out of the total 12 degrees of freedom in our calculations, only with the doubly degenerate bending modes involving the motion of the hydrogens in nonreacting CH_3 group excluded. Comparison of flux−flux autocorrelation functions obtained by using the exact dynamics method and the CC-TDSCF method shows that the CC-TDSCF method is capable of producing very accurate results. Our calculations clearly reveal that the CC-TDSCF method is a powerful approximation quantum dynamics method. It allows us to partition a big problem into several smaller ones. By changing partition systematically, one can investigate the correlations between different degrees of freedom. By grouping modes with strong correlations together as a cluster, one can systematically improve accuracy of the result.

I. Introduction

In the last 2 decades with development of various efficient representation schemes[1−3] and time propagators,[4,5] the time dependent wave packet method has became a dominant computational tool for studying complex chemical dynamics problems with more than three degrees of freedom. It has enjoyed considerable successes on accurate quantum reactive scattering studies of four-atom chemical reactions in a full six dimensions.[6−9]

The main advantage of the TD method over the traditional time-independent method is that it scales almost linearly with the number of basis functions. However, due to the quantum nature, that number of basis functions grows exponentially with dimensionality, so it is only practical at present to deal with seven to eight strongly coupled degrees of freedom.[10] Hence, to study quantum dynamical problems involving many atoms, one has to resort to the reduced dimensionality approach to cut down the number of degrees of freedom included in dynamical studies or some computational approximate methods to overcome the scaling of effort with dimensionality.

A promising approach is the time-dependent self-consistent field (TDSCF) method.[11−20] In the simplest version, i.e., the single configuration time-dependent self-consistent field (SC-TDSCF) approach, the wave function of the system is written as a direct product of the wave functions for subsystems.[11−14,16] A principal drawback of SC-TDSCF is that it replaces exact interaction between subsystems by mean-field coupling, resulting in the lack of correlations between subsystems. One way to account for the important correlations neglected in SC-TDSCF is to add wave functions with different configurations to give more flexibility to the wave function of the system, resulting in the so-called multiconfiguration time-dependent self-consistent field (MC-TDSCF) method.[17−21] Wave functions with different configurations are usually constructed by imposing orthogonal condition explicitly, making it hard to use more than a few configurations in numerical implementation. Furthermore, the resulting equations for MC-TDSCF are very complicated compared to those in SC-TDSCF method. For these reasons, MC-TDSCF has only been applied to some model problems.

The closely related multiconfiguration time-dependent Hartree method (MCTDH) generalizes MC-TDSCF in a systematic way, thus eliminating the need for choices of the TDSCF states.[22,23] It has successfully been applied to study various realistic and complex quantum dynamical problems (see ref 22 for references). Very recently, it was successfully applied to calculate the $J = 0$ cumulative reaction probability the six atom H + CH_4 reaction in full 12 dimensions on an ab initio potential energy surface (PES), from which the thermal rate constants in a broad temperature region were obtained for the reaction.[24] However, the general application of MCTDH method to strongly correlated systems yields a numerical method wherein the number of possible TDSCF configuration grows exponentially with the number of degrees of freedom, again confining practical use of the method to relatively small systems.

Recently, we proposed a new and efficient scheme for MC-TDSCF, namely, continuous-configuration time-dependent self-consistent field (CC-TDSCF) method.[25] Very often dynamical processes in polyatomic systems can be described as a system of a few strongly coupled degrees of freedom which characterize the process of interest, coupled with clusters of bath modes. Bath modes inside a cluster may be coupled to each other, but

† Part of the special issue "John C. Light Festschrift".
* Corresponding author. E-mail: zhangdh@dicp.ac.cn.
‡ National University of Singapore
§ Nanyang Technological University.
|| Chinese Academy of Sciences.

10.1021/jp0565960 CCC: $33.50
Published on Web 02/14/2006

the coupling between bath modes in different clusters may be neglected. The basic idea for our new method is to use discrete variable representation (DVR)[2] for the system and then to each DVR point of the system we associate a configuration of wave function in terms of direct product wave functions for different clusters of the bath modes. In this way, the correlations between the system and bath modes, as well as the correlations between bath modes in each individual cluster can be described properly, while the correlations between bath modes in different clusters are neglected. Since the DVRs used for the system are orthogonal, the resulting equations are as simple in structure as those for SC-TDSCF. The dimensionalities of the equations are determined by the number of degrees of freedom in the system and in each individual cluster of bath modes. The method was tested on a model problem of a one-dimensional double well linearly coupled to a harmonic bath.[26−28] It was found for this model harmonic bath system that the CC-TDSCF approach is much more accurate than the traditional SC-TDSCF method, because it allows the bath wave function to change continuously along the system coordinate, in contrast to the SC-TDSCF method which just uses one bath wave function. Our test demonstrated that the CC-TDSCF approach was capable of producing semiquantitative or even quantitative results.

In the present work we test CC-TDSCF method on the $H + CH_4 \rightarrow H_2 + CH_3$ reaction. Because of its important roles in CH_4/O_2 combustion chemistry, the reaction has been the subject of both experimental and theoretical interest for many years. Because five of the six atoms involved are hydrogens, it is an ideal candidate for high quality ab initio quantum chemistry calculations of the potential energy surface and quantum dynamics studies. This reaction has become a benchmark for developing and testing various theoretical methods to accurately study polyatomic chemical reactions.[10,29−35] Very recently, Manthe and co-workers constructed a high quality PES for the reaction in the vicinity of the saddle point. The PES can be used to calculate thermal rate constant for the reaction by using flux−flux autocorrelation-based methods.[24] The cumulative reaction probabilities for the total angular momentum $J = 0$ were calculated on the PES from which the thermal rate constants for the reaction in a broad range of temperature were obtained. It was found that the theoretical thermal rate constants has an accuracy comparable to or even exceeding experimental precision. In this work, we use the PES developed by Manthe and co-workers to test the accuracy of the CC-TDSCF method for the $H + CH_4$ reaction.

In the following section, we introduce the CC-TDSCF method in a general form and review the transition state wave packet method (TSWP). In Sec. III, we then present the results for some seven dimensional calculations and 10 dimensional calculations by using the approximation CC-TDSCF method, in comparison with the results from exact calculations. We briefly summarize in section IV.

II. Theory

A. CC-TDSCF Method. Consider a general multidimensional problem with Hamiltonian written as

$$\hat{H}(\mathbf{s}, \mathbf{x}^1, \mathbf{x}^2, ..., \mathbf{x}^N) = \hat{h}(\mathbf{s}) + \sum_i^N \hat{h}(\mathbf{x}^i) + \mathbf{V}(\mathbf{s}, \mathbf{x}^1, \mathbf{x}^2, ..., \mathbf{x}^N) \tag{1}$$

where $\mathbf{s}$ and $\mathbf{x}^i$ ($i = 1, ..., N$) are multidimensional vectors, with dimension equal to n_s and n_i, respectively. We call $\mathbf{s}$ the system coordinates, and $\mathbf{x}^i$ the ith cluster of bath coordinates. Hence the total dimension of the problem is $n_s + \sum_i^N n_i$. We partition it into an n_s dimensional system and N clusters of bath modes. In eq 1, the Hamiltonians for system $\boldsymbol{s}$ and bath cluster $\mathbf{x}^i$ are given by

$$\hat{h}(\mathbf{s}) = \sum_j^{n_s} [\hat{T}(s_j) + V(s_j)] = \sum_j^{n_s} \hat{h}(s_j) \tag{2}$$

$$\hat{h}(\mathbf{x}^i) = \sum_j^{n_j} [\hat{T}(x_j^i) + V(x_j^i)] = \sum_j^{n_j} \hat{h}(x_j^i) \tag{3}$$

where $\hat{T}$ is the kinetic energy operator, $V(x)$ is the one-dimensional reference for coordinate x.

The CC-TDSCF ansatz for the total wave function is written as follows[25]

$$\Psi(\mathbf{s}, \mathbf{x}^1, ..., \mathbf{x}^N, t) = \sum_{\alpha=1}^M C_\alpha(t) |\mathbf{s}_\alpha\rangle \Phi_\alpha(\mathbf{x}^1, ..., \mathbf{x}^N, t) \tag{4}$$

where $|\mathbf{s}_\alpha\rangle$ denotes DVR points for the system coordinates $\mathbf{s}$ which is constructed via direct product of DVR grids for individual coordinate s_i ($i = 1, ..., n_s$); $\Phi_\alpha(\mathbf{x}^1, ..., \mathbf{x}^N, t)$, which depends on the DVR point $|\mathbf{s}_\alpha\rangle$, is written as a product of single-mode functions as in the single configuration TDSCF

$$\Phi_\alpha(\mathbf{x}^1, ..., \mathbf{x}^N, t) = \prod_{i=1}^N \phi_\alpha^i(\mathbf{x}^i, t) \tag{5}$$

where $\phi_\alpha^i(\mathbf{x}^i, t)$ is the time-dependent wave function for the ith cluster of bath coordinates, $\mathbf{x}^i$, at $|\mathbf{s}_\alpha\rangle$ DVR point for the system coordinates. It has the following constraints

$$\left\langle \phi_\alpha^i(t) \middle| \frac{\partial}{\partial t} \phi_\alpha^i(t) \right\rangle = 0, \text{ and } \langle \phi_\alpha^i(0) | \phi_\alpha^i(0) \rangle = 1 \tag{6}$$

for $i = 1, 2, ..., N$. These constraints will guarantee that the single-mode functions are normalized at any time t.

Now we introduce the "single-hole function":

$$\Phi_\alpha^{(i)} = \phi_\alpha^1 ... \phi_\alpha^{(i-1)} \phi_\alpha^{(i+1)} ... \phi_\alpha^N \tag{7}$$

Then Φ_α in eq 5 can be written as

$$\Phi_\alpha = \phi_\alpha^i \, \Phi_\alpha^{(i)} \tag{8}$$

Employing the Dirac-Frenkel variational principle,[36] we can obtain the equations of motions as[25]

$$i\dot{C}_\alpha = \sum_\beta \langle \mathbf{s}_\alpha \Phi_\alpha | \hat{H} | \mathbf{s}_\beta \Phi_\beta \rangle \, C_\beta, \qquad \text{for } \alpha = 1, ..., M \tag{9}$$

$$i[\dot{C}_\alpha \, \phi_\alpha^i + C_\alpha \dot{\phi}_\alpha^i] = \sum_\beta \langle \mathbf{s}_\alpha \Phi_\alpha^{(i)} | \hat{H} | \mathbf{s}_\beta \Phi_\beta^{(i)} \rangle [C_\beta \, \phi_\beta^i] \tag{10}$$

$$\text{for } i = 1, 2, ..., N$$

By defining a new function

$$\varphi_\alpha^i = C_\alpha \, \phi_\alpha^i \tag{11}$$

we can rewrite eq 10 as

$$i\dot{\varphi}_\alpha^i = \sum_\beta \langle \mathbf{s}_\alpha \Phi_\alpha^{(i)} | \hat{H} | \mathbf{s}_\beta \Phi_\beta^{(i)} \rangle \, \varphi_\beta^i, \qquad i = 1, ..., N \tag{12}$$

The single-mode function ϕ_α^i can be obtained by multiplying

C_α^* on both sides of eq 11 and resorting the normalization conditions for the single-mode functions

$$C_\alpha^* \varphi_\alpha^i = |C_\alpha|^2 \phi_\alpha^i \rightarrow \phi_\alpha^i = \frac{C_\alpha^* \varphi_\alpha^i}{||C_\alpha^* \varphi_\alpha^i||} \tag{13}$$

where $||f|| = \sqrt{\langle f|f\rangle}$ denotes the modulo of a function.

We can see from eq 9 that the evolution of C_i in eq 9 is governed by an effective Hamiltonian arising from averaging the total Hamiltonian over all the bath modes at each DVR point in the system coordinates, while the evolution of wave function for the ith cluster of bath modes is governed by an effective Hamiltonian arising from averaging the total Hamiltonian over all the bath clusters except itself (ith mode) on each DVR point in the system coordinates. Hence to propagate the total wave function, one needs to solve an n_s dimensional equation for the system and N equations for all the N bath clusters with a dimension equal to $n_s + n_i$ for the ith cluster.

To propagate CC-TDSCF equations given in eq 9 and 12, one needs to calculate the averages of Hamiltonian over wave functions. Let us first take a look at the average in eq 12. Substituting the Hamiltonian given in eq 1 into the average, we can get

$$\begin{aligned}\langle \mathbf{s}_\alpha \Phi_\alpha^{(i)}|\hat{H}|\mathbf{s}_\beta \Phi_\beta^{(i)}\rangle &= \langle \mathbf{s}_\alpha \Phi_\alpha^{(i)}|\hat{h}(\mathbf{s}) + \sum_k^N \hat{h}(\mathbf{x}^k) + \mathbf{V}(\mathbf{s}, \mathbf{x}^1, \mathbf{x}^2, ..., \mathbf{x}^N)|\mathbf{s}_\beta \Phi_\beta^{(i)}\rangle \\ &= \langle \mathbf{s}_\alpha|\hat{h}(\mathbf{s})|\mathbf{s}_\beta\rangle\langle \Phi_\alpha^{(i)}|\Phi_\beta^{(i)}\rangle + [\sum_k^N \langle \Phi_\alpha^{(i)}|\hat{h}(\mathbf{x}^k)|\Phi_\alpha^{(i)}\rangle + \\ &\qquad \langle \Phi_\alpha^{(i)}|\mathbf{V}(\mathbf{s}_\alpha, \mathbf{x}^1, \mathbf{x}^2, ..., \mathbf{x}^N)|\Phi_\alpha^{(i)}\rangle]\delta_{\alpha,\beta} \\ &= \langle \mathbf{s}_\alpha|\hat{h}(\mathbf{s})|\mathbf{s}_\beta\rangle\langle \Phi_\alpha^{(i)}|\Phi_\beta^{(i)}\rangle + [\hat{h}(\mathbf{x}^i) + \sum_{k\neq i}^N E_\alpha^{\mathrm{eff}}(\mathbf{x}^k) + \\ &\qquad V^{\mathrm{eff}}(\mathbf{s}_\alpha, \mathbf{x}^i)]\delta_{\alpha,\beta}\end{aligned} \tag{14}$$

where

$$E_\alpha^{\mathrm{eff}}(\mathbf{x}^k) = \langle \phi_\alpha^k(\mathbf{x}^k, t)|h(\mathbf{x}^k)|\phi_\alpha^k(\mathbf{x}^k, t)\rangle \tag{15}$$

with $\phi_\alpha^k(\mathbf{x}^k, t)$ given in eq 5, is the expectation value of Hamiltonian, or, energy for ith bath cluster at the $|\mathbf{s}_\alpha\rangle$ DVR point. $V_{eff}(\mathbf{s}_\alpha, \mathbf{x}^i)$ in eq 14 is the effective potential at system DVR $|\mathbf{s}_\alpha\rangle$ and coordinates for ith bath cluster $\mathbf{x}^i$.

To discuss the first term in eq 14, we write a system DVR point $|\alpha\rangle$ as $|s_{k\mu}\rangle|\alpha^{(k)}\rangle$, with $|s_{k\mu}\rangle$ denoting the μth DVR point for kth system coordinate, $|\alpha^{(k)}\rangle$ denoting the corresponding DVR points for the other coordinates in the system. For the kth system coordinate, we have

$$\begin{aligned}\langle s_{k\mu}|\langle \alpha^{(k)}|\hat{h}(s_k)|s_{k\nu}\rangle|\beta^{(k)}\rangle\langle \Phi^{(i)}_{s_{k\mu}\alpha^{(k)}}|\Phi^{(i)}_{s_{k\nu}\beta^{(k)}}\rangle &= \\ \langle s_{k\mu}|\hat{h}(s_k)|s_{k\nu}\rangle\langle \Phi^{(i)}_{s_{k\mu}\alpha^{(k)}}|\Phi^{(i)}_{s_{k\nu}\beta^{(k)}}\rangle\delta_{\alpha^{(k)}\beta^{(k)}}\end{aligned} \tag{16}$$

Hence the $\langle \mathbf{s}_\alpha|\hat{h}(\mathbf{s})|\mathbf{s}_\beta\rangle\langle \Phi_\alpha^{(i)}|\Phi_\beta^{(i)}\rangle$ matrix is block diagonal for each system coordinate as in ordinary DVR representation. However, the matrix for each system coordinate is now time-dependent, in contrast to that in ordinary DVR representation.

Once having matrix elements for $\langle \mathbf{s}_\alpha \Phi_\alpha^{(i)}|\hat{H}|\mathbf{s}_\beta \Phi_\beta^{(i)}\rangle$, it is straightforward to do one more integration with the wave function for the ith bath cluster to get

$$\begin{aligned}\langle \mathbf{s}_\alpha \Phi_\alpha|\hat{H}|\mathbf{s}_\beta \Phi_\beta\rangle &= \langle \phi_\alpha^i|\langle \mathbf{s}_\alpha \Phi_\alpha^{(i)}|\hat{H}|\mathbf{s}_\beta \Phi_\beta^{(i)}\rangle|\phi_\beta^i\rangle \\ &= \langle \mathbf{s}_\alpha|\hat{h}(\mathbf{s})|\mathbf{s}_\beta\rangle\langle \Phi_\alpha|\Phi_\beta\rangle + [\sum_k^N E_\alpha^{\mathrm{eff}}(\mathbf{x}^k) + \\ &\qquad V^{\mathrm{eff}}(\mathbf{s}_\alpha)]\delta_{\alpha,\beta}\end{aligned} \tag{17}$$

With matrix elements for $\langle \mathbf{s}_\alpha \Phi_\alpha|\hat{H}|\mathbf{s}_\beta \Phi_\beta\rangle$ and $\langle \mathbf{s}_\alpha \Phi_\alpha^{(i)}|\hat{H}|\mathbf{s}_\beta \Phi_\beta^{(i)}\rangle$ written down, we can propagate the equations of motion for $C_\alpha(t)$ and ϕ_α^i. We use split-operator method to carry out these propagations. Everything is very straightforward, as in ordinary DVR based wave packet propagation, except that the Hamiltonians involved now are time-dependent. So we have to diagonalize relevant matrices at every step. This may produce a bottleneck for computational speed if the maximum number of DVR points used for one system coordinate becomes large. While in the current application this number is around 50, so it does not cause any problem to the computation.

B. Application to the H + CH_4 System. The thermal rate constant, $k(T)$, can be calculated from the time integral of a flux−flux autocorrelation function[37−39]

$$k(T) = Q_r(T)^{-1} \int_0^\infty dt\ \mathcal{C}_{ff}(t), \tag{18}$$

where $Q_r(T)$ is the reactant partition function

$$\mathcal{C}_{ff}(t) = tr[\hat{F}e^{i\hat{H}t_c*}\hat{F}e^{-i\hat{H}t_c}] = \sum_{n=0} \mathcal{C}_{ff}^n(t), \tag{19}$$

and $t_c = t - i\beta/2$ with $\beta = (k_B T)^{-1}$. $\mathcal{C}_{ff}^n$ is defined as the autocorrelation function for the nth transition state wave packet.[37] In present study, we focus on the flux−flux autocorrelation function for its ground transition state wave packet[37]

$$C_{ff}(t) = \mathcal{C}_{ff}^0(t) = \langle \psi_g(t)|\hat{F}|\psi_g(t)\rangle \tag{20}$$

The wave function $\psi_g(t)$ for the ground-state transition state wave packet is given by

$$\psi_g(t) = e^{-i\hat{H}t}e^{-\hat{H}\beta/2}\sqrt{\lambda}|+\rangle|g_0(\mathbf{s}')g_1(\mathbf{x}^1)...g_N(\mathbf{x}^N)\rangle, \tag{21}$$

where $|g_k(\mathbf{x}^k)\rangle$ ($k = 1, 2, ..., N$) is the ground-state wave function for $h_k(\mathbf{x}^k)$, $|+\rangle$ is the flux operator eigenfunction with nonzero eigenvalue of λ for coordinate perpendicular to the dividing surface in system, $|g_0(\mathbf{s}')\rangle$ is the ground-state wave function on the dividing surface $\mathbf{s}'$. From eq 21, one can see that we first propagate each transition state wave packet in imaginary time to $\beta/2$, and then propagate it in real time.

Following Manthe and co-workers,[24,29,30] we use transition state normal coordinate system in our calculation to minimize correlation effects in the transition state region. Normal modes and normal coordinates were calculated at the transition state geometry and the corresponding linear transformation matrix was used throughout the calculation to convert the working coordinates into Cartesian coordinates. The transition state for the reaction, $H_a-H_b-CH_3$, is of C_{3v} symmetry with H_a-H_b-C lying on the C_{3v} symmetry axis. Here we labeled two hydrogen atoms involving in reaction to distinguish them from three other hydrogen atoms in the CH_3 group. For such a system of six atoms, there are 12 normal vibrational modes. They are the imaginary mode (Q_1) concerning the asymmetric stretching motion of the $H_a-H_b-CH_3$ fragments on the C_{3v} symmetry axis, a doubly degenerate low-frequency bending modes (Q_2, Q_3) mainly involving the motion of H_a atom, an umbrella mode (Q_4) for the nonreacting CH_3 group, a doubly degenerate high-

frequency bending modes (Q_5, Q_6) mainly involving the motion of H_b atom, another doubly degenerate bending modes (Q_7, Q_8) essentially involving the motion of the hydrogens in nonreacting CH_3 group, a symmetric stretching mode (Q_9) of the $H_a-H_b-CH_3$ fragments on the C_{3v} symmetry axis, and a symmetric (Q_{10}) and doubly degenerate asymmetric stretches (Q_{11},Q_{12}) concerning mainly the nonreacting CH_3 group. Among all these modes, Q_1 and Q_9 are directly relevant to the reaction.

With mixed derivatives in the kinetic energy resulting from vibrational angular momentum neglected, the Hamiltonian for the system can be simply written as

$$\hat{H}(Q_1, Q_2, ..., Q_{12}) = \sum_{i=1}^{12} -\frac{1}{2}\frac{\partial^2}{\partial Q_i^2} + \mathcal{V}(Q_1, Q_2, ..., Q_{12})$$

$$= \sum_{i=1}^{12} h_i(Q_i) + V(Q_1, Q_2, ..., Q_{12}) \qquad (22)$$

where

$$h_i(Q_i) = -\frac{1}{2}\frac{\partial^2}{\partial Q_i^2} + V_i(Q_i) \qquad (23)$$

is the one-dimensional Hamiltonian for these normal modes. The reference potential $V_i(Q_i)$ for mode i is taken as

$$V_i(Q_i) = 0, \quad \text{for } Q_1, Q_4, \text{ and } Q_9$$

$$V_i(Q_i) = \mathcal{V}(Q_1 = 0, ..., Q_i, ..., Q_{12} = 0),$$

for other coordinates.

To choose a proper dividing surface, we define two new coordinates Q'_1 and Q'_9 by rotating Q_1 and Q_9 coordinates by an angle $\theta = 25°$

$$Q'_1 = \sin\theta\, Q_1 + \cos\theta\, Q_9$$

$$Q'_9 = \cos\theta\, Q_1 - \sin\theta\, Q_9.$$

The dividing surface is located as $Q'_1 = 0$ in our calculation.

III. Results

A. Numerical Details. To check the accuracy of the CC-TDSCF method, we need to calculate the autocorrelation functions by using exact quantum dynamics method. With the computer available to us, we are able to include up to 10 of out the total 12 degrees of freedom. Intensive tests reveal that the doubly degenerate bending modes (Q_7, Q_8) involving the motion of the hydrogens in nonreacting CH_3 group essentially play no role in the dynamics, hence are excluded in this study. We use 49 sine-DVR in a range of [−120, 120] for Q_1, 13 sine-DVR in a range of [−100,50] for Q_4, 29 sine-DVR in a range of [−50, 150] for Q_9. For Q_2, Q_3, Q_5, Q_6, Q_{11}, and Q_{12}, we use five potential optimized DVR (PODVR),[40] and for Q_{10}, we use six PODVR. Hence the basis number used in the exact ten-dimensional quantum dynamics calculation reaches 1.7×10^9. The temperature considered in this study is 500 K. We propagate wave packet 50 steps for imaginary time propagation in eq 21. For real time propagation, the time step is 5 au for the exact calculation and 1 au for the CC-TDSCF method because of the self-consistent nature of the method.

B. Seven-Dimensional (7D) Results. We first test the CC-TDSCF method on seven low-frequency modes, i.e., Q_1, Q_2, Q_3, Q_4, Q_5, Q_6, and Q_9. In the CC-TDSCF calculation, we choose Q_1 and Q_9 as the system coordinates **s**. The other five coordinates involved, Q_2, Q_3, Q_4, Q_5, Q_6, are treated as five bath clusters, i.e., with one coordinate in every bath cluster. In the paper, we use {(1, 9),(2),(3),(4),(5),(6)} to denote this kind of partition in coordinates, with the numbers in the first pair of parentheses referring the system coordinates, and the number(s) in the following pairs of parentheses referring the coordinate(s) in each bath cluster. Under this partition, one needs to solve one two-dimensional equation for the system, plus five three-dimensional equations for the bath clusters.

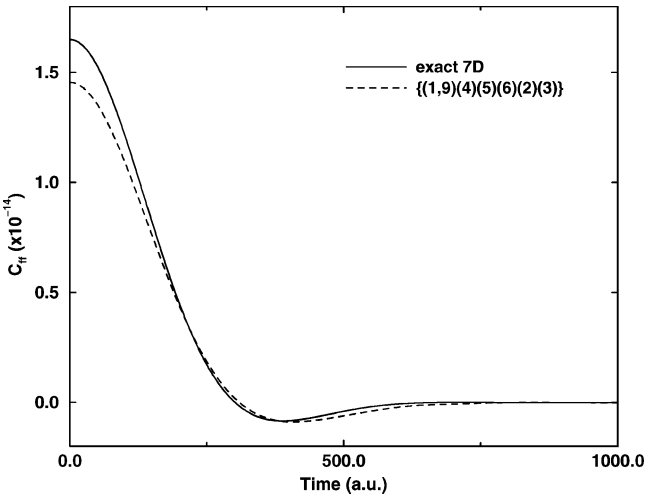

Figure 1. C_{ff} as a function of real time propagation for the ground transition state by using both exact quantum method and CC-TDSCF method with Q_1, Q_2, Q_3, Q_4, Q_5, Q_6, Q_9 included in calculations.

Figure 1 shows C_{ff} as a function of real time propagation, t, for the ground transition state by using both exact quantum method and CC-TDSCF method. The exact C_{ff} shown in Figure 1 exhibits a typical behavior for the flux−flux autocorrection function for a direct reaction: it decays quickly as time increases, goes through zero at $t \sim 300$ au, then becomes a little bit negative, and finally gets stabilized at zero at $t \sim 700$ au. Hence for the temperature considered here, recrossing in flux−flux autocorrection does occur, although it is not substantial. From Figure 1, we can see that overall agreement between the CC-TDSCF C_{ff} and the exact one is quite good. At $t = 0$, it is about 12% smaller than the exact C_{ff}. It decays slightly slower than the exact C_{ff}, hence crosses with the exact C_{ff} curve at $t \sim 220$ au. The CC-TDSCF C_{ff} also moves in and out of the recrossing region slightly slower than the exact one.

It is quite interesting to see that the largest difference between CC-TDSCF and exact C_{ff} is at $t = 0$, right after the imaginary time propagation. Neglecting of correlations between bath modes prevent the whole system from relaxing as in the exact treatment during imaginary time propagation, making the CC-TDSCF C_{ff} at $t = 0$ smaller than the exact one. While during the real time propagation, neglecting of correlations between bath modes makes the whole system slower in dissipating energy and in moving away from the dividing surface. As a result, the CC-TDSCF C_{ff} decays slightly slower than the exact one as shown in Figure 1.

Figure 2 shows the exact and CC-TDSCF C_{fs} as a function of time by integrating the C_{ff} function shown in Figure 1. The curves looks very similar, except that the CC-TDSCF C_{fs} is lower than the exact one. At $t \sim 300$ au when they reach their maximum values, the CC-TDSCF C_{fs} is about 9% smaller than the exact one. The difference increases to 12% at $t \sim 700$ au when they are stabilized. Thus, the CC-TDSCF method intro-

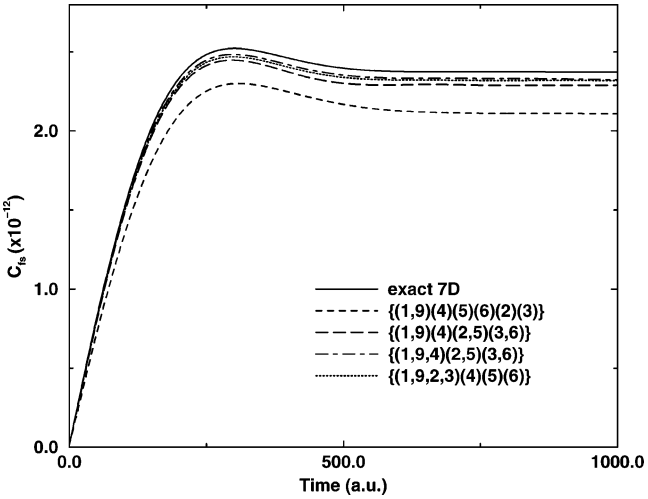

Figure 2. C_{fs} as a function of real time propagation for the ground transition state by using both exact quantum method and CC-TDSCF method with Q_1, Q_2, Q_3, Q_4, Q_5, Q_6, and Q_9 included in the calculations.

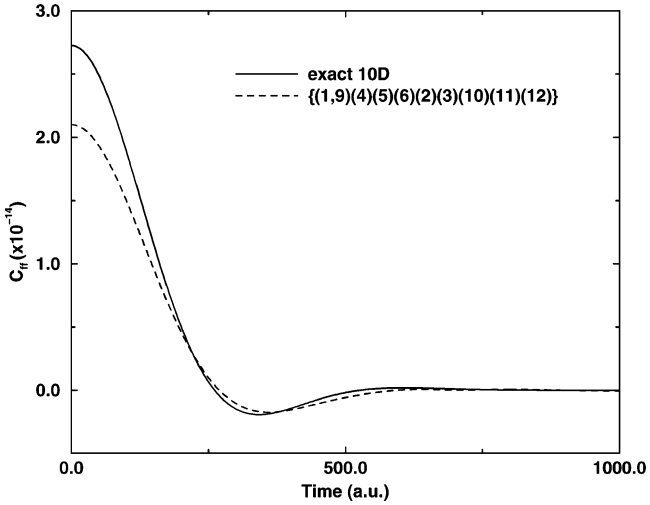

Figure 3. Same as Figure 1, except with three high-frequency modes, Q_{10}, Q_{11}, and Q_{12}, included.

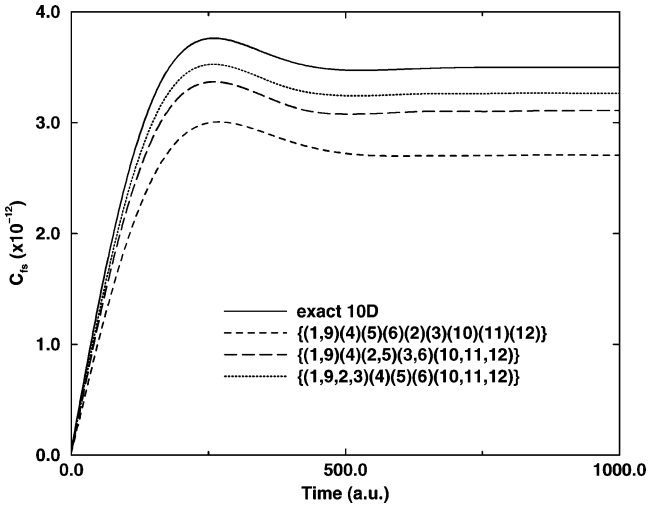

Figure 4. Same as Figure 2, except with three high-frequency modes, Q_{10}, Q_{11}, and Q_{12}, included.

duces an error of 12% by approximating a seven-dimensional problem with one two-dimensional plus five three-dimensional problems.

Under the {(1, 9),(2),(3),(4),(5),(6)} partition, we only took into account the correlations between system coordinates and individual bath coordinate, while neglected the correlations between bath coordinates. To investigate the importance of the correlations between bath coordinates, we carried out many calculations by using different partition of the coordinates. It was found that the H_a bending modes Q_2 and Q_3 have substantial correlations with the H_b bending modes Q_5 and Q_6 on the same plane, i.e., Q_2 correlates Q_5, Q_3 correlates with Q_6. Thus, an higher accuracy may be achieved by putting Q_2 and Q_5 in one bath cluster, Q_3 and Q_6 in another bath cluster. As we can see from Figure 2 that CC-TDSCF C_{fs} with the {(1, 9),(4),(2, 5),(3, 6)} partition is considerably more accurate than that with the {(1, 9),(2),(3),(4),(5),(6)} partition, when compared to the exact result. It is only smaller than the exact result by 3.5%. Under this partition, one needs to solve one two-dimensional equation for the system, one three-dimensional equation for Q_4, two four-dimensional equations for (Q_2, Q_5) and (Q_3, Q_6). If we put the umbrella mode Q_4 in the system, i.e., with a {(1, 9, 4),(2, 5),(3, 6)} partition, we can further reduce the difference between the CC-TDSCF and exact C_{fs} to 2%. As we can see from Figure 2 that the CC-TDSCF C_{fs} with the {(1, 9, 4),(2, 5),(3, 6)} partition is essentially identical to the exact one, indicating that there is very little correlation between (Q_2, Q_5) and (Q_3, Q_6) clusters. Another way to improve the accuracy of the {(1, 9),(4),(2, 5),-(3, 6)} partition is to move Q_2 and Q_3 modes to the system, resulting a {(1, 9, 2, 3),(4),(5),(6)} partition. Figure 2 shows that the accuracy of the {(1, 9, 2, 3),(4),(5),(6)} partition is very close to that of the {(1, 9, 4),(2, 5),(3, 6)} partition. Compared to the {(1, 9),(4),(2, 5),(3, 6)} partition, the {(1, 9, 4),(2, 5),(3, 6)} partition takes into account the correlations between Q_4 mode and Q_2, Q_3, Q_5, Q_6 modes, while the {(1, 9, 2, 3),(4),-(5),(6)} partition takes into account the correlation between Q_4 mode and Q_2, Q_3 modes, the correlations between Q_2 and Q_6, Q_3 and Q_5. The close agreement between the {(1, 9, 4),(2, 5),-(3, 6)} partition and the {(1, 9, 2, 3),(4),(5),(6)} partition indicates to some extent that the correlation between Q_4 mode and Q_2, Q_3 modes are more important than the correlation between Q_4 mode and Q_5, Q_6 modes.

C. Ten Dimensional (10D) Results. Figure 3 and Figure 4 shows C_{ff} and C_{fs}, respectively, as a function of real time propagation, t, for the ground transition state by using both exact quantum method and CC-TDSCF method with Q_{10}, Q_{11}, and Q_{12} included in dynamical calculations. Before comparing the exact 10D result with the CC-TDSCF ones, let us make a comparison between the 7D and 10D exact results shown in Figures 1 and 3. In our calculations, we set the ground-state energy for every degree of freedom included in the calculation to be zero. Hence, if a degree of freedom plays no role to the dynamics, C_{ff} will only change very little (due to potential average effect) when that degree of freedom is included in dynamics calculations. Figure 3 show that the exact C_{ff} changes substantially when Q_{10}, Q_{11}, and Q_{12} are included in dynamical calculation. At $t = 0$, the 10D C_{ff} in Figure 3 is larger than 7D C_{ff} in Figure 1 by about 60%. For the corresponding C_{fs} shown in Figure 2 and Figure 4, the 10D C_{fs} is about 50% larger than the 7D C_{fs}. It is well-known that there is some kind of mixing between these stretching modes and the umbrella mode in normal coordinates, in particular at geometries far way from the reference geometry. Hence freezing stretch modes as in the 7D calculation may substantially underestimate C_{fs}, as discussed by Miller and co-workers in the H_2 + OH system.[41]

As in the 7D case shown in Figure 1, we carried out a CC-TDSCF calculation with a {(1, 9),(2),(3),(4),(5),(6),(10),(11),-(12)} partition. The comparison between the exact 10D C_{ff} and the CC-TDSCF one shown in Figure 3 is very similar to that in

Figure 1, except that the difference between these two curves increases. At $t = 0$, the exact one is larger than the CC-TDSCF one by 22%. Consequently, the difference in C_{fs} between them shown in Figure 4 also increases compared to that in 7D. When stabilized, the exact C_{fs} is about 22% larger than the CC-TDSCF one. Thus, these three high frequencies modes also have some strong correlations with themselves or other modes. Once again, we can see that the CC-TDSCF C_{ff} decays slower than the exact one as in 7D case, and it becomes slightly larger than the exact one at $t \sim 230$ au for the reason discussed.

As in 7D calculations shown in Figure 2, bath modes are combined together as clusters to take into account the correlations between them. One partition we tried is {(1, 9),(4),(2, 5),(3, 6),(10, 11, 12)} following the 7D calculation, with additional three high frequencies modes put in one cluster. As we can see from Figure 4 that the {(1, 9),(4),(2, 5),(3, 6),(10, 11, 12)} partition is considerably more accurate than the {(1, 9),(2),(3),(4),(5),(6),(10),(11),(12)}. It cuts the error of the later partition by half to about 11%, compared to the exact result. But this error is obviously larger than that of 3.5% for the {(1, 9),(4),(2, 5),(3, 6)} partition, indicating Q_{10}, Q_{11}, and Q_{12} modes not only correlate among themselves, they also correlate to other modes.

After intensive tests, we found that Q_{10}, Q_{11}, and Q_{12} also correlate with Q_2 and Q_3 modes. Since $Q_2(Q_3)$ correlates with Q_4, Q_5, Q_6 modes to some extent, one way to take into account all the correlations Q_2 and Q_3 have with Q_4, Q_5, Q_6, Q_{10}, Q_{11}, and Q_{12} modes is to put Q_2 and Q_3 in the system, resulting in a {(1, 9, 2, 3),(4),(5),(6),(10, 11, 12)} partition. Under this partition, one needs to solve one four-dimensional equation for the system, three five-dimensional equation for Q_4, Q_5, and Q_6, and one seven-dimensional equation for Q_{10}, Q_{11}, and Q_{12}. It sounds quite expansive to solve these equations, but compared to solving the original ten-dimensional equation, the computational efforts involved here is substantially reduced because the number of basis used in the exact 10D calculations is $13 \times 5 \times 5 = 325$ times larger than that for the seven-dimensional equation. For the basis set used in this study, the CC-TDSCF calculation is about a factor of 10 faster than the exact one. As we can see from Figure 4 that the CC-TDSCF C_{fs} with the {(1, 9, 2, 3),(4),(5),(6),(10, 11, 12)} partition agrees with the exact one rather well. It is only smaller than the exact one by 6% at $t = 700$ au.

IV. Conclusions

We calculated the flux−flux autocorrelation functions for the $H + CH_4$ reaction by using the exact quantum dynamics method and CC-TDSCF method on the potential energy surface recently developed by Manthe and co-workers. Since Q_7 and Q_8 are not important to the dynamics, we did not include them in present study. For the remaining 10 modes, we carried two sets of calculations, one with seven low-frequency modes, Q_1-Q_6, and Q_9 included, the other including all these 10 modes.

Comparison of flux−flux autocorrelation functions obtained by using the exact dynamics method and the CC-TDSCF method revealed that the CC-TDSCF method is capable of producing very accurate results. For the 7D case, the largest difference between the exact one and the CC-TDSCF one is 12% when the five bath modes were treated as five bath clusters in the {(1, 9),(2),(3),(4),(5),(6)} partition. This error was reduced to 3.5% when the {(1, 9),(4),(2, 5),(3, 6)} partition was employed. The CC-TDSCF method gave an error of 2% with the {(1, 4, 9),(2, 5),(3, 6)} partition. When the three high-frequency modes Q_{10}, Q_{11}, and Q_{12} were included in dynamics calculations, a simple {(1, 9),(2),(3),(4),(5),(6),(10),(11),(12)} partition gave an error of 22%, indicating these three high-frequency modes have some strong correlations among themselves and/or with other bath modes. By using a {(1, 9),(4),(2, 5),(3, 6),(10, 11, 12)} partition, we can reduce the error to 11%. The error can be reduced further to 6% by putting Q_2 and Q_3 in the sytem in a {(1, 9, 2, 3),(4),(5),(6),(10, 11, 12)} partition.

All these calculations clearly showed that the CC-TDSCF method is a very powerful approximation quantum dynamics method. It allows us to partition a big problem into several smaller ones. By changing partition systematically, one can investigate the correlations between different degrees of freedom. By grouping modes with strong correlations together as a cluster, one can systematically improve accuracy of the result. And, by choosing the system and bath clusters carefully, one can always keep the number of dimensions in CC-TDSCF within the computational power one has available.

Acknowledgment. The authors would like to thank Prof. Manthe for sending us the potential energy surface used in this study. This work is supported in part by Academic Research Grant R-151-000-037-112, National University of Singapore.

References and Notes

(1) Light, J. C.; Hamilton, I. P.; Lill, J. V. *J. Chem. Phys.* **1985**, *82*, 1400.
(2) Bačić, Z.; Light, J. C. *Annu. Rev. Phys. Chem.* **1989**, *40*, 469.
(3) Kosloff, R. *J. Phys. Chem.* **1988**, *92*, 2087.
(4) Fleck, J. A., Jr.; Morris, J. R.; Feit, M. D. *Appl. Phys* **1976**, *10*, 129.
(5) Tal-Ezer, H.; Kosloff, R. *J. Chem. Phys.* **1984**, *81*, 3967.
(6) Zhang, D. H.; Collins, M. A.; Lee, S.-Y. *Science* **2000**, *290*, 961.
(7) Zhang, D. H.; Yang, M.; Lee, S.-Y. *Phys. Rev. Lett.* **2002**, *89*, 103201.
(8) Zhang, D. H.; Xie, D.; Yang, M.; Lee, S.-Y. *Phys. Rev. Lett.* **2002**, *89*, 283203.
(9) Althrope, S. C.; Clary, D. C. *Annu. Rev. Phys. Chem.* **2003**, *54*, 493.
(10) Yang, M.; Zhang, D. H.;.; Lee, S.-Y. *J. Chem. Phys.* **2002**, *117*, 9539.
(11) Heller, E. J. *J. Chem. Phys.* **1975**, *64*, 63.
(12) Harris, R. *J. Chem. Phys.* **1980**, *72*, 1776.
(13) Gerber, R. B.; Buch, V.; Ratner, M. A. *J. Chem. Phys.* **1982**, *77*, 3022.
(14) Gerber, R. B.; Ratner, M. A. *Adv. Chem. Phys.* **1988**, *70*, 97.
(15) Messina, M.; Coalson, R. D. *J. Phys. Chem.* **1989**, *90*, 4015.
(16) Jungwirth, P.; Gerber, R. B. *Chem. Rev.* **1999**, *99*, 1583.
(17) Kosloff, R.; Hammerich, A. D.; Ratner, M. A. In *Large finite systems, Proceedings of the Twentieth Jerusalem Symposium of Quantum Chemistry and Biochemistry*; Jortner, J., Ed.; Reidel: Dordrecht, The Netherlands, 1987.
(18) Makri, N.; Miller, W. H. *J. Chem. Phys.* **1987**, *87*, 5781.
(19) Kotler, Z.; Nitzan, A.; Kosloff, R. *Chem. Phys. Lett.* **1988**, *153*, 483.
(20) Hammerich, A. D.; Kosloff, R.; Ratner, M. A. *Chem. Phys. Lett.* **1990**, *171*, 97.
(21) Wang, L.; McCoy, A. B. *J. Chem. Phys.* **2000**, *113*, 10605.
(22) Beck, M. H.; Jackle, A.; Worth, G. A.; Meyer, H.-D. *Phys. Rep.* **2000**, *324*, 1.
(23) Meyer, H.-D.; Manthe, U.; Cederbaum, L. S. *Chem. Phys. Lett.* **1990**, *165*, 73.
(24) Wu, T.; Werner, H.-J.; Manthe, U. *Science* **2005**, *306*, 2227.
(25) Bao, D. H. Z. W.; Yang, M.; Lee, S.-Y. *J. Chem. Phys.* **2005**, *122*, 024505.
(26) Zwanzig, R. *J. Stat. Phys.* **1973**, *9*, 215.
(27) Caldeira, A. O.; Leggett, A. J. *Ann. Phys. (N.Y.)* **1983**, *149*, 374.
(28) Topaler, M.; Makri, N. *J. Chem. Phys.* **1994**, *101*, 7500.
(29) H-Larranaga, F.; Manthe, U. *J. Chem. Phys.* **2000**, *113*, 5115.
(30) Bowman, J. M.; Wang, D.; Huang, X.; H−Larranaga, F.; Manthe, U. *J. Chem. Phys.* **2001**, *114*, 9683.
(31) Wang, M. L.; Zhang, J. Z. H. *J. Chem. Phys.* **2001**, *114*, 7013.
(32) Wang, M. L.; Li, Y.; Zhang, J. Z. H.; Zhang, D. H. *J. Chem. Phys.* **2000**, *113*, 1802.
(33) Wang, M. L.; Zhang, J. Z. H. *J. Chem. Phys.* **2002**, *117*, 3081.
(34) Wang, D. Y.; Bowman, J. M. *J. Chem. Phys.* **2001**, *115*, 2055.

(35) Takayanagi, T. *J. Chem. Phys.* **1996**, *104*, 2237.
(36) Frenkel, J. *Wave Mechanics*; Clarendon Press: Oxford, U.K., 1934.
(37) Zhang, D. H.; Light, J. C.; Lee, S. Y. *J. Chem. Phys.* **1999**, *111*, 5741.
(38) Wang, H.; Thoss, M.; Miller, W. H. *J. Chem. Phys.* **2000**, *112*, 47.
(39) Yamamoto, T.; Wang, H.; Miller, W. H. *J. Chem. Phys.* **2002**, *116*, 7335.
(40) Echave, J.; Clary, D. C. *Chem. Phys. Lett.* **1992**, *190*, 225.
(41) Manthe, U.; Seideman, T.; Miller, W. H. *J. Chem. Phys.* **1994**, *101*, 4759.